Article

Research on Acoustic Emission Characteristics and Crack Evolution during Rock Failure under Tensile and Tensile- and Compressive-Shear Stress States

Yifan Xu [1] , Jie Hu [2,*], Peng He [1], Gang Wang [3] and Haolan Pan [2,*]

[1] College of Civil Engineering and Architecture, Shandong University of Science and Technology, Qingdao 266590, China; yifan.xu@sdust.edu.cn (Y.X.)
[2] School of Mechanical Engineering, Nanjing University of Science and Technology, Nanjing 210094, China
[3] Department of Civil Engineering, Fujian University of Technology, Fuzhou 350118, China; wanggang23611@163.com
* Correspondence: jie.hu@njust.edu.cn (J.H.); panhl99@163.com (H.P.)

Abstract: Tensile, compressive-shear, and tensile-shear failure are three typical failure modes of rock- and lining-support structural materials in underground engineering. Comparative studies of the acoustic emission (AE) evolution characteristics of specimens of the same shape and size under different stress states are of great significance in determining universal disaster warning guidelines. Based on a self-developed multi-functional test system, direct tensile, compressive-shear, and tensile-shear tests were conducted on intact and jointed rock-like specimens, comparing AE amplitude and peak frequency parameters under different failure modes from the perspectives of crack scale and crack type evolution. All failure tests were monitored with microcrack propagation at an early stage until ultimate rupture occurred at the peak-load moment. As a result, the "quiet-period" could only be observed from the compressive-shear test. The AE signals distributed in three bands can be used as an indicator of failure identifications. Tensile and shear cracks can be identified by strong and weak amplitudes of low- and high-frequency signals. These results enhance the knowledge of the failure modes of rock mechanics for more applications in monitoring disasters in rock engineering.

Keywords: acoustic emission; rock-like specimen; tensile test; tensile-shear test; compressive-shear test

1. Introduction

As underground engineering has progressed to vast and burial depths and spans, the stress state of the rock mass has become more complex. Rock mass collapses are common, with tensile, compressive-shear, and tensile-shear failure being three common failure types [1]. Mechanical fatigue can be viewed as a process of gradual accumulation of damage in rock specimens under stress or strain, a process that leads to changes in the structure and properties of rock specimens and the creation and expansion of cracks and fractures [2]. When an external load is applied to a rock specimen, it generates stresses in different directions, and these stresses, when reaching their limit values, cause small cracks or deformations inside the specimen [3,4], which results in the generation of AE signals. Laboratory testing is an essential tool for investigating rock failure processes. The use of AE monitoring during testing to assess the elastic wave signals of internal rupture of rock specimens or rock-like specimens can efficiently predict the evolutionary stage of specimen failure, providing a theoretical foundation for disaster monitoring and early warning [5]. There have been many valuable studies on the AE evolution of specimens during direct tensile and compressive-shear failure compared to tensile-shear failure [6–11] but few reports on the AE evolution of rock specimens of the same shape and size under direct tensile, tensile-shear, and compressive-shear failure modes. Experimental investigations on tensile-shear failure have primarily focused on the analysis of specimen rupture characteristics

and the formulation of strength requirements [12,13], but the depth is insufficient in studies on the evolution of AE signals during failure.

At present, there is no research on quantitative frequency non-band classification methods for different rock samples. Previous researchers mainly determined the frequency characteristics of rock acoustic emission signals by band distribution, and most of the previous studies showed that rock acoustic emission signals present multi-band characteristics [9,11,12], and the specific values should be divided into three or five bands according to the nature of the rock samples, which is a hierarchical distribution characteristic. Different rocks and rock samples have different frequency-band distributions [8,14], which do not allow diverse frequency clustering analysis. This method is currently used more in the field of geotechnical testing, but the use of frequency-band classification is sufficient to reflect the frequency characteristics.

AE signal analysis primarily consists of parametric and waveform analysis. The former describes the features of AE signals using a set of simplified waveform parameters, such as count, energy, amplitude, duration, etc. [15]. The latter refers to selecting appropriate signal-processing methods for AE signal time-domain waveforms to obtain AE signal characteristics, such as Fourier transform-based spectral analysis, time-domain analysis, etc. [16]. The amplitude is an essential characteristic feature of the AE waveform, reflecting the maximum amplitude in the signal decay waveform, which can reflect the magnitude of the AE signal and is frequently used to perform a preliminary crack scale assessment [17]. In many cases, the study of the key physical variables characterizing the AE signal from the frequency domain is more effective and intuitive in reflecting the information and occurrence mechanism of rock fracture [18] than the research of AE waveform features in the time domain. Many scholars have paid close attention to rock failure spectral features study recently. Li [19] discovered that the AE spectrum of marble failure tests was characterized by an apparent double peak frequency (PF) independent of the test method and that the double peak frequency could represent two separate microfracture forms of the rock. Chen [6] found that the AE signals of the rock bridge in direct shear testing were dispersed in high- and low-frequency bands and that the dispersion of the peak frequency band to the medium frequency could be used as crucial rock failure precursor information. Through the uniaxial compression test of fractured mortar rock specimens, Guo [14] discovered that the AE signals of the specimen failure revealed three distinct peak frequency bands: high, medium, and low. Zhao [20] found that the AE signals were dispersed in three frequency bands and studied how the frequency bands evolved at different loading stages. According to the findings of this study, a combination of AE and other characteristics can be utilized to thoroughly assess the presence of macroscopic rupture, boosting the accuracy of early warning of rock failure. As previously stated, little research has been conducted on the evolution of the amplitude and peak frequency distributions of tensile and tensile-shear failure. It is unknown whether similar patterns exist in tensile and tensile-shear experiments. Furthermore, it is evident that low-amplitude AE signals correspond to small-scale cracks, and high-amplitude AE signals belong to large-scale rupture. However, the link between the magnitude of the signal at the peak AE frequency and the crack types is more complex and has yet to be determined [19,21,22], and more research is required.

To explore the AE characteristics and crack evolution of the same shape and size of rock specimens under three stress states, direct tensile, compressive-shear, and tensile-shear tests were performed on intact and jointed cubic cement mortar specimens utilizing self-developed multifunctional test equipment. AE monitored the interior cracking in specimens. AE amplitude and peak frequency were analyzed to understand crack sizes and types under different failure modes. We classified the internal crack types of the specimens using the conventional RA (rising time/max. amplitude)–AF (average frequency, ring down count/duration)-based method and compared the results with the newly proposed amplitude–PF-based method to provide new ideas for analyzing microscopic cracks and macroscopic ruptures in the failure process.

2. Test Procedures

2.1. Specimen Preparation

The type of rock samples used in the experiments in this paper, the selection of rock sample materials and the reasons for it, the size of rock samples, and the preparation process are consistent with the results of previous research [23], so they will not be described in detail; detailed information can be found in that study. The rock-like specimen preparation process is shown in Figure 1b. The mechanical parameters are tested and shown in Table 1.
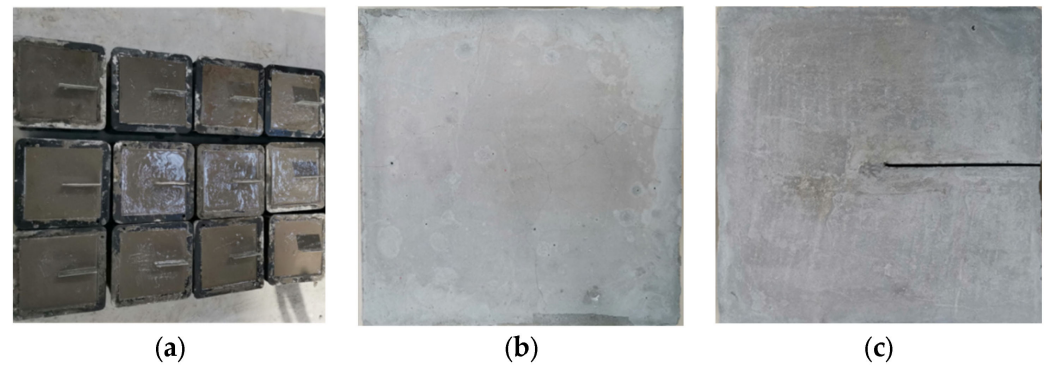

| (a) | (b) | (c) |

Figure 1. Rock-like material specimens. (**a**) The preparation process; (**b**) the intact specimen; (**c**) the specimen with a joint persistence of 50%.

Table 1. Mechanical properties of the rock-like materials.

Uniaxial Compressive Strength (MPa)	Uniaxial Tensile Strength (MPa)	Elastic Modulus (GPa)	Poisson's Ratio	Rock Cohesion (MPa)	Internal Friction Angle of Rock (°)
18.29	0.77	4.76	0.18	5.45	36.5

2.2. Test and Monitoring Methods

Direct tensile, tensile-shear, and compressive-shear tests were performed using a self-developed multifunctional test system [24]. This work tested six sets of specimens, and the test conditions are provided in Table 2. A normal tensile force was applied to the specimen in the direct tensile tests, and the specimen was loaded at a rate of −0.5 kN/s until failure. The compressive-shear tests and the tensile-shear tests, which were conducted under constant normal stress of 5 MPa and −0.15 MPa respectively, corresponded to roughly 20% of the uniaxial compressive and tensile strength of specimens, respectively. The usual load was applied at a loading rate of 0.5 kN/s. When the normal load reached the preset value, the specimen was loaded laterally with displacement control at a rate of 1 mm/min until it broke.

Table 2. Test conditions.

Test Type	Rock Specimen Number	Normal Stress/MPa	Joint Persistence (JP)
Tensile test	T1	/	0%
	T2	/	50%
Tensile-shear test	TS1	−0.15	0%
	TS2	−0.15	50%
Compressive-shear test	CS1	5	0%
	CS2	5	50%

This study employed a PAC Express-8 AE instrument to monitor the AE signals. The monitoring system can achieve a 16-bit resolution at a sampling rate of up to 10 MSPS. The monitoring system uses an AE sensor (Nano-30) that has an operating frequency range of 150–400 kHz, with a resonance frequency of around 300 kHz and a frequency variation of

around 20 kHz. The couplers used were those supplied by Physical Acoustics USA, which were ideally suited to the task. The specimen's back surface had an AE transducer attached to it, which touched the specimen through a coupling agent and was held in place by tape. Acquisition of the AE data as well as filtering and postprocessing of the signals were performed on an AE mainframe supplied by Physical Acoustics USA, which has its own filtering capabilities and analytical functions such as AE amplitude and peak frequency analysis. The sampling frequency was 2 MHz, and the threshold value was 40 dB. Figure 2 depicts the test and monitoring equipment.
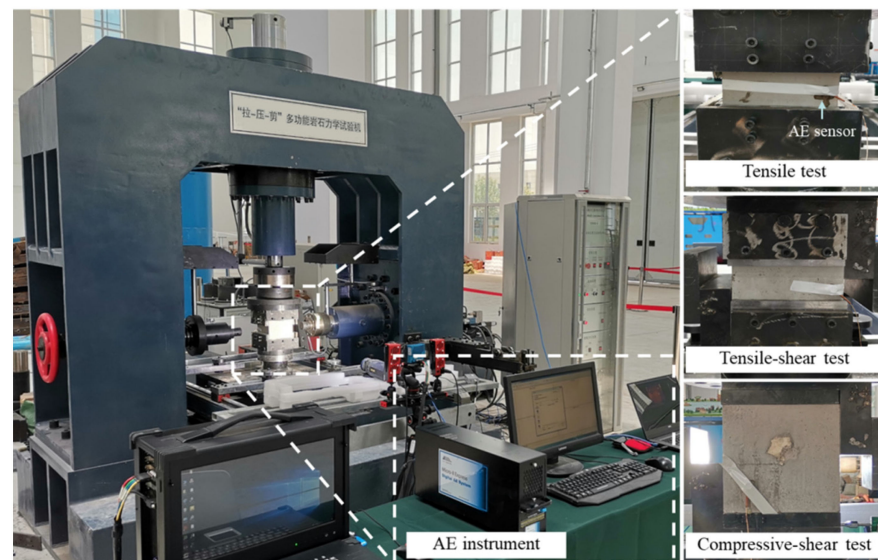

Figure 2. The test and monitoring equipment (The name of the equipment is "Tension-Compression-Shear" multifunctional rock mechanics testing machine).

3. Results Analysis

3.1. AE Amplitudes

The AE amplitude evolution characteristics of intact specimens and jointed specimens from different types of tests were compared. Considering the difference in loading time between the various tests, the ratio of loading to peak load (σ/σ_{peak}) was used as the horizontal axis for the unified comparative analysis of the three tests, with a minimum scale value of 0.1 σ_{peak}.

In the tensile test, the peak stress of the intact specimen was 0.75 MPa, and the number of AE events to peak stress was 85,634. In the compressive-shear test, the peak stress of the intact specimen was 11.24 MPa, and the number of AE events to peak stress was 3645. In the tensile-shear test, the peak stress of the intact specimen was 2.76 MPa, and the number of AE events to peak stress was 94,865. In the tensile test, the peak stress of the jointed specimen was 0.34 MPa, and the number of AE events at peak stress was 16,253. In the compression-shear test, the peak stress of the jointed specimen was 6.53 MPa, and the number of AE events at peak stress was 16,103. In the tension-shear test, the peak stress of jointed specimen was 1.66 MPa, and the number of AE events at peak stress was 36,972. A comparison of the AE amplitude distribution versus loading stress level for the three types of tests is shown in Figure 3.

From Figure 3a,b, it can be seen that the amplitude distribution in tensile tests is relatively scattered, ranging from 40 to 100 dB, and the pattern is the same for intact and jointed specimens. From 20% σ_{peak} to 60% σ_{peak}, the AE amplitude is mainly between 40 and 55 dB, and there are sporadic AE signals with a high amplitude of 55~80 dB, indicating that the crack scale is small at the early stage of loading, and micro-cracking is predominant. From 60% σ_{peak} to 80% σ_{peak}, the AE signals are abundant. However, the amplitude remains primarily between 40 and 55 dB, but the number of signals with high amplitudes larger than 55 dB increases significantly, and there are signals with high amplitudes larger than

90 dB in the intact specimen at this stage, indicating that large-scale cracks have begun to appear. The number of cracks is significantly increased. After 80% σ_{peak}, the AE amplitude is more evenly distributed in the range of 40~75 dB, with sporadic, very-high-amplitude signals, indicating that the number of microcracks in the specimen has been significantly reduced, and large-scale fractures have formed.
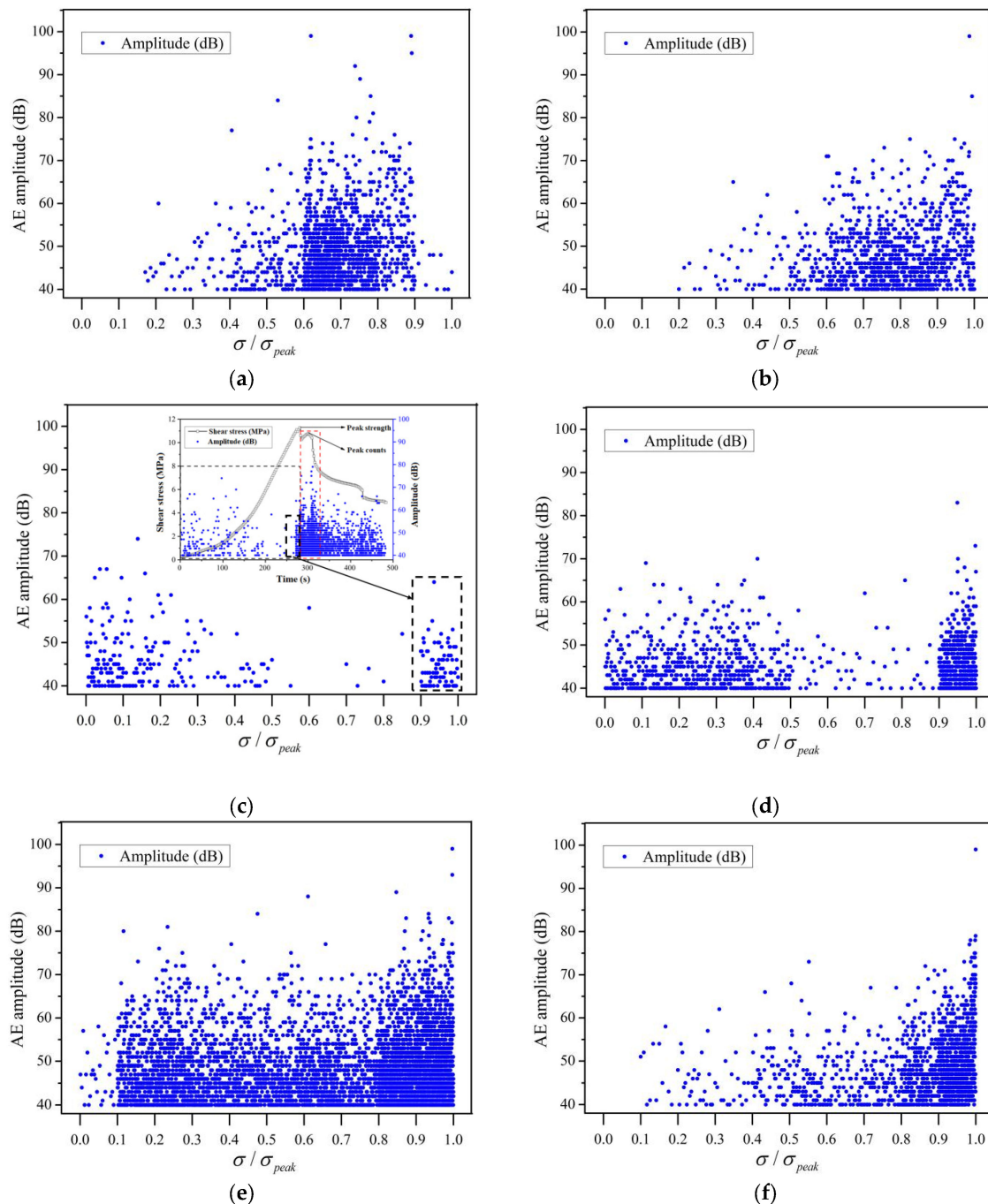

Figure 3. AE amplitude distribution characteristics in three test types. (**a**) Specimen T1; (**b**) specimen T2; (**c**) specimen CS1; (**d**) specimen CS2; (**e**) specimen TS1; (**f**) specimen TS2.

The distribution of AE signals of compressive-shear failure before the peak strength is primarily in the range of 40–55 dB, which is substantially less than tensile failure, showing that small-scale microcracks are prominent in the compressive-shear stress state (Figure 3c,d). Few AE signals between 55 and 70 dB exist at the early loading stage and near the peak strength. It is worth noting that the peak strength does not coincide with

the maximum AE counts, and the macroscopic shear fracture surface has not yet been pierced. The difference in the distribution pattern of AE signals between intact and jointed specimens in the tensile-shear test is more significant than in the previous two types of shear tests, as shown in Figure 3e,f. The intact specimen's amplitude distribution is primarily in the 40~70 dB region, with similar amplitude distribution characteristics at different loading moments. The amplitude distribution of the jointed specimen is similar to that of the tensile test, with AE amplitudes mainly ranging from 40 to 55 dB before 90% σ_{peak}, with few signals of high amplitude between 55 and 80 dB, indicating that the crack scale is generally small and dominated by microcracks. In contrast, the number of high-amplitude signals increases significantly at the peak strength moment.

Comparing the amplitude distributions of the three tests, it can be seen that there is a precise "quiet period" in the AE signals of compressive-shear failure compared to failure due to tensile and tensile-shear forces. The different tests all reflect the failure evolution pattern of the accumulation of small-scale micro-cracks at the beginning of loading until the large-scale rupture near the peak strength moment. The amplitude distribution of tensile-shear failure in the intact specimen is somewhat similar to that of compressive-shear failure. In contrast, the amplitude distribution of tensile-shear failure in the jointed specimen is more similar to that of tensile failure.

3.2. AE Peak Frequency

For the three types of tests, the AE waveforms of the different tests were extracted, the FFT spectra of all the AE signals of the various tests were transformed, and the peak frequency distributions were counted. The maximum values of the peak frequencies of the AE signals of the three tests did not exceed 500 kHz, and the distribution of the peak frequencies of the different tests showed a three-band distribution. Based on the clustering characteristics of the peak frequency values, the AE signals below 50 kHz were classified as a band of low frequencies, 50~200 kHz as a band of medium frequencies, and above 200 kHz as a high-frequency band. The distribution of the peak frequency bands and the percentages of the three types of tests as the stress is continuously loaded are shown in Figure 4. In the tensile test, only low-frequency signals are generated until 60% σ_{peak} of the intact rock specimen. Only sporadic medium- and high-frequency signals are generated in the jointed specimen at this stage. In contrast, near the failure, the medium- and high-frequency signals of the intact and jointed specimens start to increase. In particular, only medium-frequency signals are generated during the 90~100% σ_{peak} loading interval for the intact specimen. In the compressive-shear test, the high-frequency signals are mainly generated in the initial loading stage, and the intact rock specimen has relatively more medium-frequency signals, accounting for 60.1%. In contrast, the jointed specimen still has mainly low-frequency signals, and both specimens have significantly more medium- and low-frequency signals near the failure. In the tensile-shear test, both specimens generate three frequency bands of signals throughout the loading process. The proportion of high-frequency signals is much greater than in the tension and compression-shear tests. However, all three tests are similar in that the number of medium-frequency signals increases significantly near the moment of failure, which can be an essential precursor to identifying failure.

The peak frequencies of the jointed specimens under the three types of failure are selected for moving average processing (step size of 50) to investigate the evolution of the peak frequency distribution of the three types of testing. The peak frequencies of the three types of tests fluctuate and decrease with stress loading. The tensile and tensile-shear tests have similar patterns, with peak frequencies decreasing in the early loading stage and fluctuating in the medium and late stages. The compressive-shear test differs significantly from the other two tests because the peak frequency fluctuates considerably at the beginning of loading. In contrast, the peak frequency values are lower near the failure time and only fluctuate within a small range. There is currently no consensus on the relationship between tensile and shear cracking and the peak frequency. As the failure mechanism of compressive-shear tests has been studied more in previous research,

the relationship between the peak frequency and cracks in compressive-shear tests was analyzed first. Liu [25] concluded that the early and medium stages of compressive-shear failure in jointed specimens are dominated by small-scale tensile cracks, with tensile cracks converging near the failure time and failing the bridge in the form of shear rupture. Combined with the peak frequency evolution features of the jointed specimen in Figure 5b, it was deduced that AE signals with high peak frequency belong to tensile cracks and those with low peak frequency correspond to shear cracks, but this is simply a qualitative conclusion. It is impossible to determine the quantitative division criteria between high and low frequencies, but it is clear from Figure 5 that the peak frequencies are above 50 kHz at the beginning of all three types of test loading. Further analysis of Figure 4d shows that there is also a large amount of signals within the low-frequency range at the beginning of the compressive-shear test of the jointed specimen. Hence, it was initially inferred that the medium- and high-frequency bands (PF ≥ 50 kHz) mainly correspond to tensile cracks, while the low-frequency band (PF < 50 kHz) should contain both tensile cracks and shear cracks. The difference between shear and tensile cracks in low-frequency bands was examined in connection with AE amplitude characteristics.
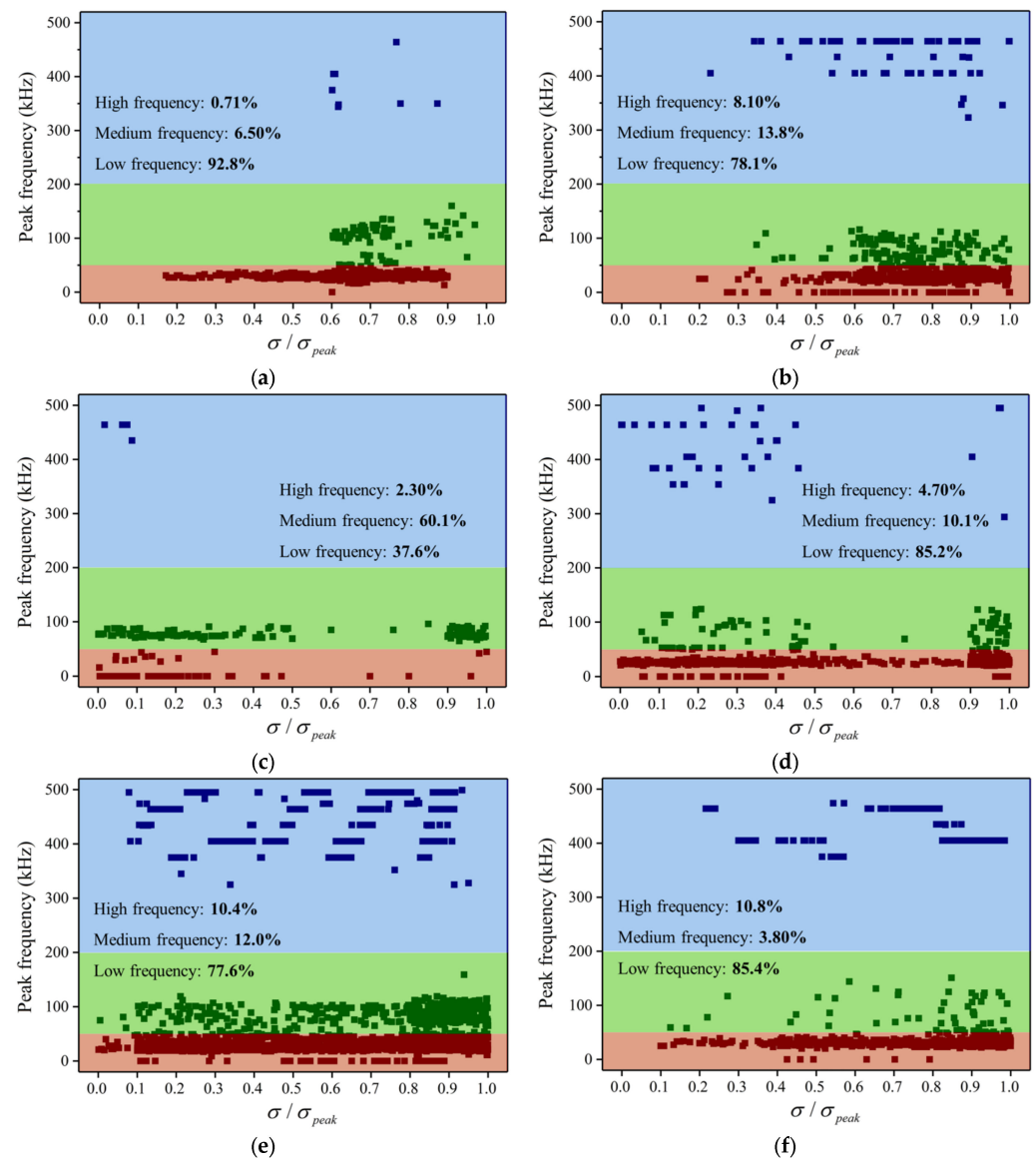

Figure 4. Peak frequency distribution characteristics in three test types. (**a**) Specimen T1; (**b**) specimen T2; (**c**) specimen CS1; (**d**) specimen CS2; (**e**) specimen TS1; (**f**) specimen TS2.
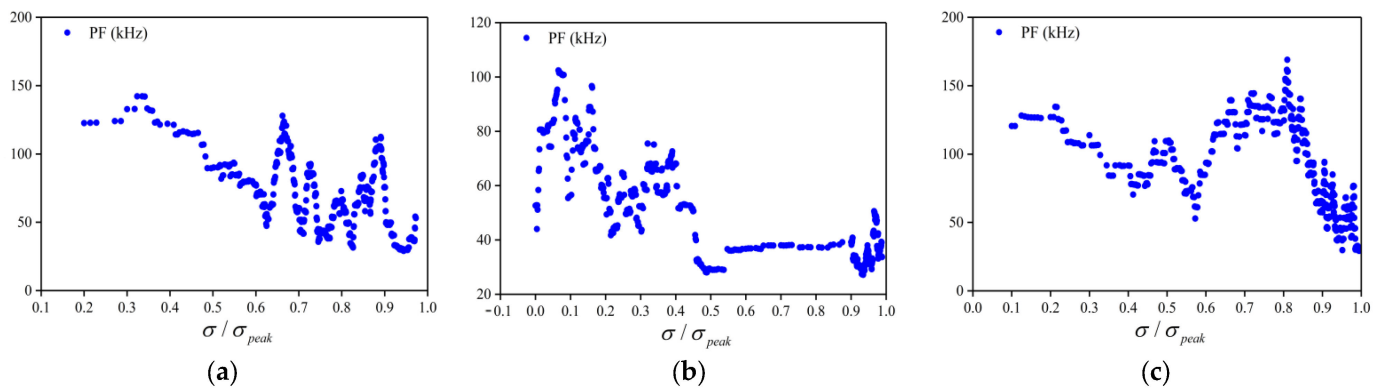
Figure 5. Peak frequency distribution characteristics of AE signal in three types of tests (moving average 50). (**a**) Specimen T2; (**b**) specimen CS2; (**c**) specimen TS2.

3.3. Classification of Crack Types

The magnitude of the shear crack is more significant than the tensile crack, and the AE amplitude can represent the crack scale. Therefore, a preliminary classification might be based on the amplitude for the co-existence of tensile and shear cracks in the low peak frequency band. After combining all the AE signals from the six experiments, the amplitude distribution statistics were determined for the medium- and high-frequency bands. In the low-frequency band, as seen in Figure 6, according to the prior analysis, it can be shown that 55 dB is a critical threshold value for the assessment of the crack scale. In the medium- and high-frequency bands, the percentage of AE signals with an amplitude below 55 dB is around 86.5%, whereas in the low-frequency band, the percentage is about 81.1%. The signals with low amplitude account for a more significant percentage, and the high-amplitude signal in the low-frequency band accounts for a more substantial percentage than that in the medium- and high-frequency band. Depending on the crack mode, crack-extension incidence produces different AE signals. Crack-extension modes involving relative motion of the two sides of the crack produce AE waveforms with short rise times and high frequencies. In contrast, shear cracks typically produce waveforms with lower frequencies and longer rise times, in other words, higher amplitudes [26]. Therefore, those with higher amplitudes in the lower-frequency range are shear cracks, and the rest of the signal then becomes tensile cracks. We considered signals with amplitudes ≥55 dB in the low-frequency band as shear cracks and other signals as tensile cracks. This rule was used to classify the crack types in each of the six tests.
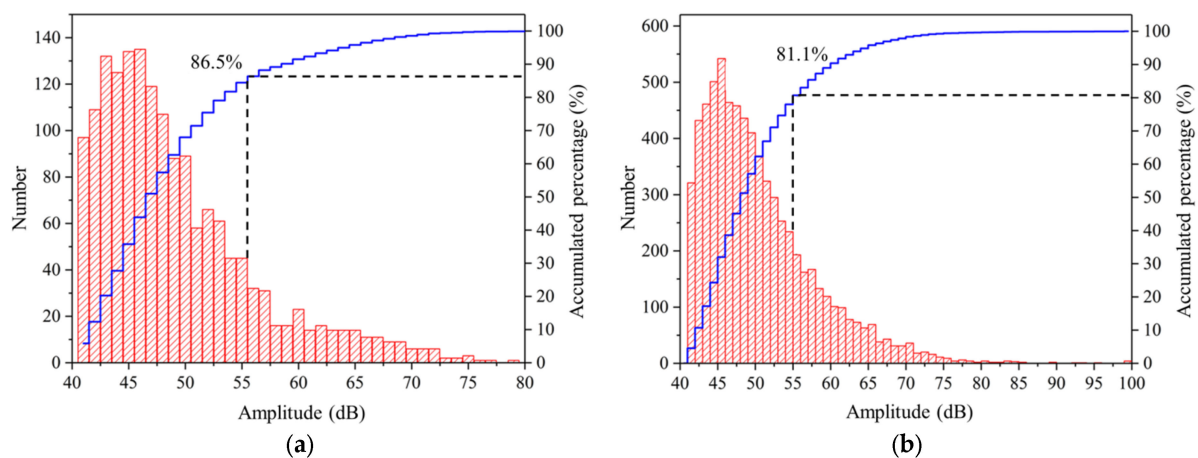

Figure 6. Amplitude distribution characteristics in medium- and high-frequency bands and low-frequency band. (**a**) Medium- and high-frequency bands; (**b**) low-frequency band.

To verify the reliability of the crack classification method based on AE amplitude and peak frequency, the RA–AF value-based method recommended by the JCMS-III B5706 was further adopted for crack classification [27]. The calculation method of RA and AF values and the crack classification principle are shown in Figure 7. Different types of crack propagation produce different waveform characteristics. Cracks appear far from the tip under tension, resulting in a shorter rise time, and the AE waveform that was collected has a higher frequency. Compared to tensile cracks, shear cracks look like longer energy waves, which produce signals with longer rise times and lower frequencies. Tensile cracks therefore generally have high AF values and low RA values, while shear cracks are the opposite. Based on this method, the crack types of the above six groups of tests were divided, as shown in Figure 8. The RA and AF values were calculated using a moving average of more than 50 counts (moving average). It should be noted that the RA–AF-based method is also an empirical discrimination method. The tensile and shear crack classification results are not entirely accurate and cannot identify the tensile-shear mixed cracks. Still, the results of existing studies show that it can meet the needs of analyzing the evolution and percentage of various kinds of cracks in the process of rock failure.
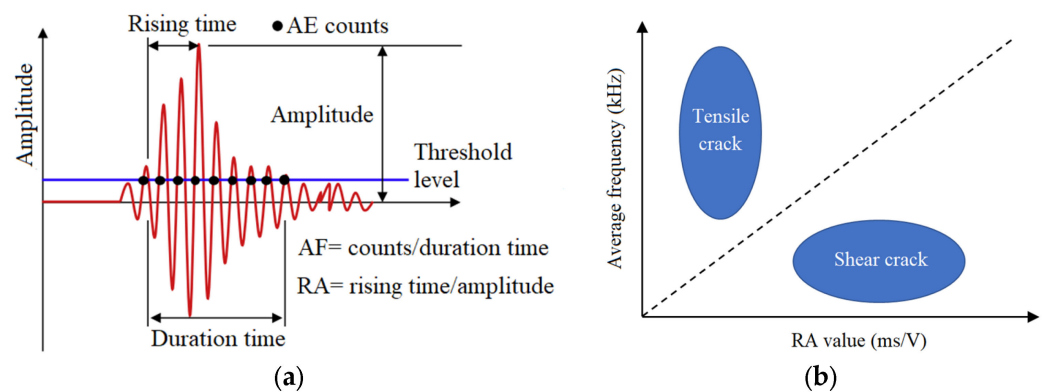

Figure 7. The classification principle of crack types. (**a**) The calculation method of RA and AF value; (**b**) crack classification based on RA–AF values.

Table 3 displays the crack categorization findings based on the two approaches. The percentage of shear cracks obtained by the two methods is significantly different for T1 and TS1, −30.5% and 9.8%, respectively. However, for the other four tests, the classification results of the two methods are consistent within 5%. This confirms the logic of the correspondence between frequency bands and crack types, as mentioned previously. There are some empirical factors that impact the determination of the split line equation by the RA–AF method due to the considerable inaccuracies in the T1 and TS1 conditions. The diagonal split line method is recommended in engineering for convenience. Still, it essentially reflects the concept of clustering, in which data points with the same characteristics are grouped into one category, and the split line should be determined based on the distribution characteristics of the actual RA–AF value data points. Farhidzadeh et al. [28], for example, employed machine learning to discover the splitting equation that is not over the origin, as illustrated in Figure 9a. Similarly, the fraction of shear cracks in the T1 condition can vary greatly when alternative splitting line formulae are used, as illustrated in Figure 9b. The dense distribution of data points near the diagonal line in Figure 8a and the forced diagonal division will undoubtedly lead to misjudgment of crack types in the T1 condition, whereas the blue splitting line in Figure 9b is certainly more reasonable, and the percentage of shear cracks identified based on this splitting line is 25.1%, which is close to the 21.5% obtained using the amplitude–PF method. Despite the absence of horizontal shear stress, the number of shear cracks in the direct tensile test is greater than in compressive-shear and tensile-shear failure tests. This is mainly because, due to material heterogeneity, the path of crack initiation may not be perpendicular to the direction of tensile stress, resulting in shear cracking, as observed in the direct tensile tests conducted by Nguyen-Tat [29] and Kourk-

oulis [9]. In summary, peak frequencies during specimen failure exhibit a "three-band" distribution, with medium- and high-frequency bands corresponding to tensile cracks and the low-frequency band containing both tensile and shear cracks, which can be roughly judged based on amplitude, i.e., AE signals with amplitudes larger than 55 dB correspond to shear cracks, and the rest correspond to tensile cracks.
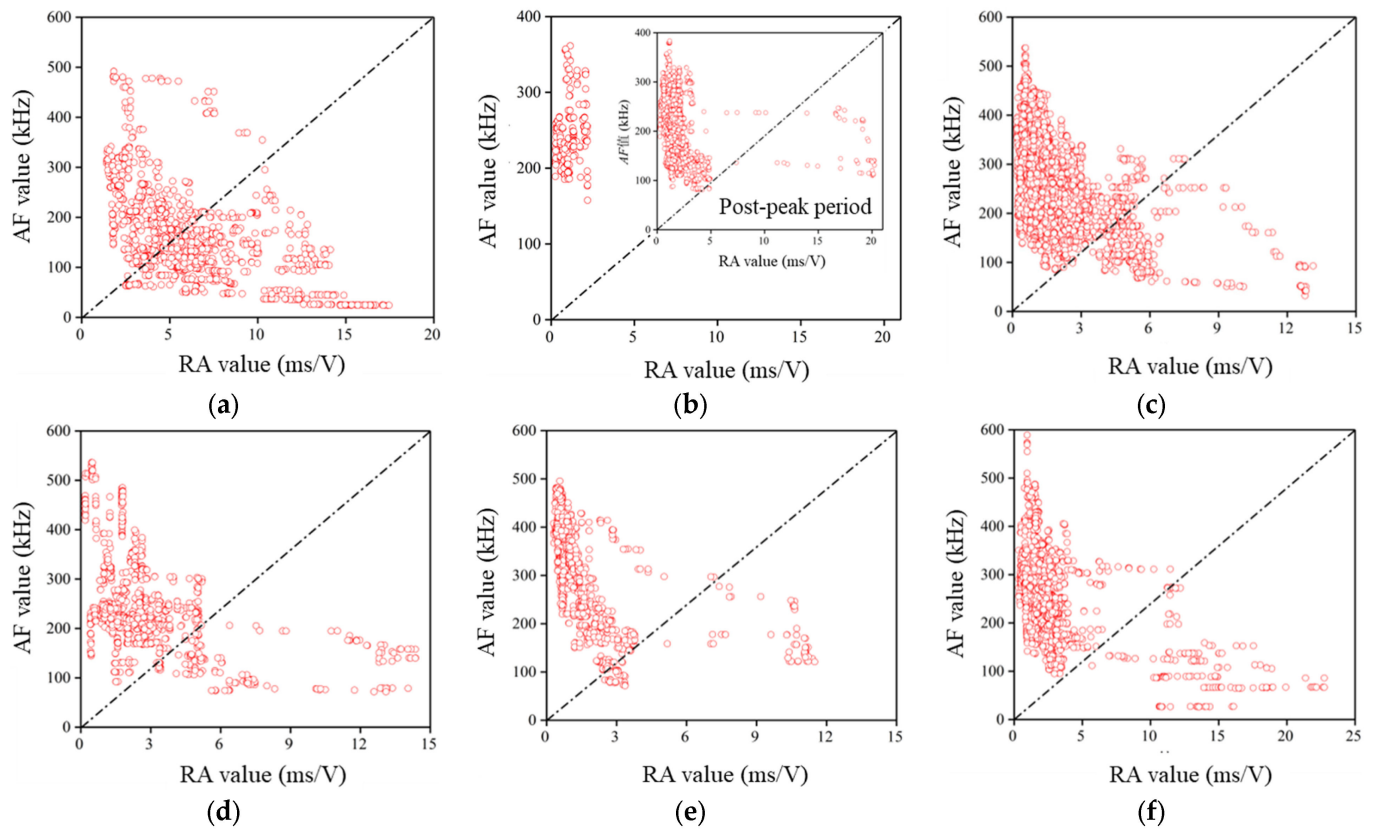

Figure 8. Crack classification based on the RA–AF values at the peak strength time. (**a**) Specimen T1; (**b**) specimen CS1; (**c**) specimen TS1; (**d**) specimen T2; (**e**) specimen CS2; (**f**) specimen TS2.

Table 3. Comparison of crack classification results between the *RA–AF* and *amplitude–PF* methods.

| Test Type	Specimen Number	Classification Method	Tensile Crack Percentage	Shear Crack Percentage	Shear Cracks' Percentage Error
Tensile test	T1	*RA–AF*	48.0%	52.0%	−30.5%
		Amplitude–PF	78.5%	21.5%	
	T2	*RA–AF*	82.5%	17.5%	−0.6%
		Amplitude–PF	83.1%	16.9%	
Compressive-shear test	CS1	*RA–AF*	100%	0.0%	3.2%
		Amplitude–PF	96.8%	3.2%	
	CS2	*RA–AF*	91.9%	8.1%	0.8%
		Amplitude–PF	91.1%	8.9%	
Tensile-shear test	TS1	*RA–AF*	93.0%	7.0%	9.8%
		Amplitude–PF	83.2%	16.8%	
	TS2	*RA–AF*	87.9%	12.1%	4.4%
		Amplitude–PF	83.5%	16.5%	
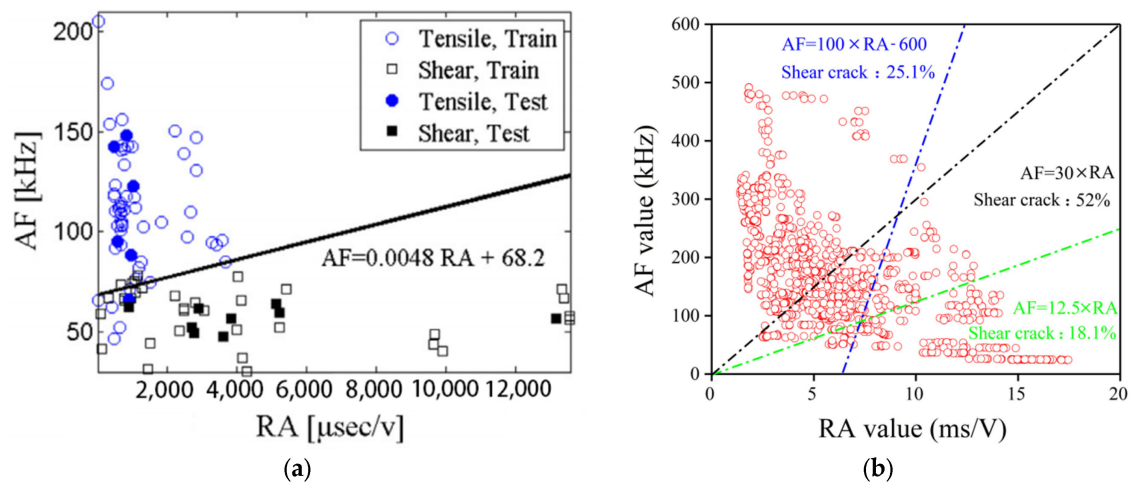
Figure 9. Determination of the secant line equation. (**a**) A diagram of secant lines that do not pass through the origin [28]; (**b**) crack classification results; (**b**) crack classification results based on different secant line equations (take the T1 as an example).

4. Conclusions

Direct tensile, tensile-shear, and compressive-shear tests were performed on rock-like specimens utilizing a self-developed multi-functional test equipment, focused on AE amplitude and peak frequency evolution during failure. Based on AE amplitude and peak frequency, the percentage of tensile and shear cracks at peak strength moments was estimated. The results were compared with RA–AF-based classification results. A summary of specific conclusions is as follows:

(1) AE signals from compressive-shear failure have a "quiet period phenomenon" compared to tensile and tensile-shear failure. The different tests reflect the failure evolution pattern of accumulation of small-scale microcracks at the beginning of loading until the large-scale rupture near the peak strength moment. In intact specimens, tensile-shear failure amplitude distribution is similar to compressive-shear failure, but in jointed specimens, it is more similar to tensile failure; this is due to the presence of tensile stresses. The specimens of both test loading methods are initially almost in the elastic deformation stage, with little damage and few cracks produced;

(2) Low-frequency signals dominate at the beginning of loading in tensile tests, but medium- and high-frequency signals grow towards failure. In compressive-shear tests, high-frequency signals are generated at the start of stress and increase towards failure. During tensile-shear tests, all three bands continuously provide signals. All three test types show an increase in mid-frequency signals near failure, which can be utilized to predict failure;

(3) The moving average of peak frequencies data demonstrate that the overall trend of the peak frequencies of the three test types fluctuates and decreases as the stresses are loaded, with the tensile and tensile-shear tests following similar patterns. The compressive-shear test varies from the other two in that the peak frequency fluctuates considerably at the beginning of loading but stabilizes towards failure;

(4) Medium- and high-frequency bands generally correlate to tensile cracks, whereas low-frequency bands comprise both tensile and shear cracks. Tensile cracks produce signals with low frequency and low amplitude, whereas shear cracks produce signals with low frequency and high amplitude. The amplitude–PF and RA–AF crack classification results were in accord. Even though there was no horizontal shear stress in the direct tensile test, shear cracks were more common. Because the material is non-homogeneous, crack-sprouting paths may not be perpendicular to tensile stress, generating shear cracks.

References

1. Hu, J.; Li, S.; Liu, H.; Li, L.; Shi, S.; Qin, C. New modified model for estimating the peak shear strength of rock mass containing nonconsecutive joint based on a simulated experiment. *Int. J. Geomech.* **2020**, *20*, 04020091. [CrossRef]
2. Sosnovskiy, L.A.; Sherbakov, S.S.; Khonsari, M.M.; Bogdanovich, A.V. From fatigue and tribology to tribo-fatigue. *Int. J. Mater. Struct. Integr.* **2021**, *14*, 164–237. [CrossRef]
3. Shcherbakov, S.S. Modeling of the damaged state by the finite-element method on simultaneous action of contact and noncontact loads. *J. Eng. Phys. Thermophys.* **2012**, *85*, 472–477. [CrossRef]
4. Shcherbakov, S.S. State of volumetric damage of tribo-fatigue system. *Strength Mater.* **2013**, *45*, 171–178. [CrossRef]
5. Bian, C.; Wang, J.Y.; Guo, J.Y. Damage mechanism of ultra-high performance fibre reinforced concrete at different stages of direct tensile test based on acoustic emission analysis. *Constr. Build. Mater.* **2021**, *267*, 120927. [CrossRef]
6. Chen, G.Q.; Sun, X.; Wang, J.C.; Wang, D.; Zhu, Z. Detection of cracking behaviors in granite with open precut cracks by acoustic emission frequency spectrum analysis. *Arab. J. Geosci.* **2020**, *13*, 258. [CrossRef]
7. Chen, W.C.; Chen, L.H.; Chen, Y.C. Using a novel shear apparatus coupled with acoustic emission to investigate shear fracture evolution of cement-based materials in macro- and micro-views. *Constr. Build. Mater.* **2018**, *187*, 665–673. [CrossRef]
8. Du, K.; Li, X.F.; Wang, S.; Tao, M.; Li, G.; Wang, S. Compressive-shear failure properties and acoustic emission (AE) characteristics of rocks in variable angle shear and direct shear tests. *Measurement* **2021**, *183*, 109814. [CrossRef]
9. Kourkoulis, S.K.; Pasiou, E.D.; Dakanali, I.; Stavrakas, I.; Triantis, D. Notched marble plates under direct tensile: Mechanical response and fracture. *Constr. Build. Mater.* **2018**, *167*, 426–439. [CrossRef]
10. Shang, D.L.; Chen, Y.D.; Zhao, Z.H.; Shangguan, S.; Qi, X. Mechanical behavior and acoustic emission characteristics of intact granite undergoing direct shear. *Eng. Fract. Mech.* **2021**, *245*, 107581. [CrossRef]
11. Wang, J.Y.; Guo, J.Y. Damage investigation of ultra high performance concrete under direct tensile test using acoustic emission techniques. *Cem. Concr. Compos.* **2018**, *88*, 17–28. [CrossRef]
12. Chen, J.; Zhou, H.; Zeng, Z.Q.; Lu, J. Macro- and microstructural characteristics of the tension-shear and compressive-shear fracture of granite. *Rock Mech. Rock Eng.* **2020**, *53*, 201–209. [CrossRef]
13. Huang, D.; Cen, D.F.; Song, Y.X. Comparative investigation on the compressive-shear and tension-shear behaviour of sandstone at different shearing rates. *Rock Mech. Rock Eng.* **2020**, *53*, 3111–3131. [CrossRef]
14. Guo, K.L.; Yang, L.; Sheng, X.C.; Mei, J.; Xiang, L.B.; Zhang, B.; Yang, W.M.; Song, G.X. Fracture mechanical behavior and AE characteristics of rock-like material containing 3-D crack under hydro-mechanical coupling. *Rock Soil Mech.* **2019**, *11*, 4380–4390. (In Chinese)
15. Das, A.K.; Suthar, D.; Leung, C.K.Y. Machine learning based crack mode classification from unlabeled acoustic emission waveform features. *Cem. Concr. Res.* **2019**, *121*, 42–57. [CrossRef]
16. Kumar, C.V.; Vardhan, H.; Murthy, C.S.; Karmakar, N.C. Estimating rock properties using sound signal dominant frequencies during diamond core drilling operations. *J. Rock Mech. Geotech.* **2019**, *11*, 850–859. [CrossRef]
17. Yang, J.; Mu, Z.L.; Yang, S.Q. Experimental study of acoustic emission multi-parameter information characterizing rock crack development. *Eng. Fract. Mech.* **2020**, *232*, 107045. [CrossRef]
18. Jiang, R.C.; Dai, F.; Liu, Y.; Li, A.; Feng, P. Frequency characteristics of acoustic emissions induced by crack propagation in rock tensile fracture. *Rock Mech. Rock Eng.* **2021**, *54*, 2053–2065. [CrossRef]
19. Li, L.R.; Deng, J.H.; Zheng, L.; Liu, J.F. Peak frequency characteristics of acoustic emissions in white marble during direct tensile tests. *Rock Mech. Rock Eng.* **2017**, *50*, 1337–1346. [CrossRef]

20. Zhao, K.; Yang, D.; Gong, C.; Zhuo, Y.; Wang, X.; Zhong, W. Evaluation of internal microcrack evolution in red sandstone based on time-frequency domain characteristics of acoustic emission signals. *Constr. Build. Mater.* **2020**, *260*, 120435. [CrossRef]

21. Ban, Y.X.; Fu, X.; Xie, Q.; Zhou, X. Evaluation of fracture morphology of shale in Brazilian tests and analysis of power spectral characteristics. *Chin. J. Geotech. Eng.* **2019**, *41*, 2307–2315. (In Chinese)

22. Zhang, Y.B.; Liang, P.; Yao, X.L.; Sun, L.; Tian, B.-Z.; Liu, X.-X. Experimental study of energy and frequency characteristics of acoustic emissions induced from tensile and shear cracks in tunnel rockburst process. *Eur. J. Environ. Civ. Eng.* **2020**, *26*, 3961–3980. [CrossRef]

23. Hu, J.; Wang, M.; Rong, X.; Wang, X.; Xiong, Z.; Shi, S. Influences of Joint Persistence on the Compressive-Shear and Tensile-Shear Failure Behavior of Jointed Rock Mass: An Experimental and Numerical Study. *Rock Mech. Rock Eng.* **2023**, *56*, 8151–8165. [CrossRef]

24. Li, S.; Hu, J.; Amann, F.; Li, L.; Liu, H.; Shi, S.; Hamdi, P. A multifunctional rock testing system for rock failure analysis under different stress states: Development and application. *J. Rock Mech. Geotech.* **2022**, *14*, 1531–1544. [CrossRef]

25. Liu, Y.M.; Xia, C.C. Study of models and strength behavior of rock mass containing discontinuous joints in direct shear. *Chin. J. Geotech. Eng.* **2006**, *28*, 1242–1247. (In Chinese)

26. Aggelis, D.G.; Matikas, T.E.; Shiotani, T. Advanced acoustic techniques for health monitoring of concrete structures. In *The Song's Handbook of Concrete Durability*; Kim, S.H., Ann, K.Y., Eds.; Middleton Publishing, Inc.: London, UK, 2010; pp. 331–378.

27. *JCMS-IIIB5706*; Japan Construction Material Standards. Monitoring Method for Active Cracks in Concrete by Acoustic Emission. The Federation of Construction Material Industries: Kumamoto, Japan, 2003.

28. Farhidzadeh, A.; Mpalaskas, A.C.; Matikas, T.E.; Farhidzadeh, H.; Aggelis, D.G. Fracture mode identification in cementitious materials using supervised pattern recognition of acoustic emission features. *Constr. Build. Mater.* **2014**, *67*, 129–138. [CrossRef]

29. Nguyen-Tat, T.; Ranaivomanana, N.; Balayssac, J.P. Identification of tensile failure in concrete by Acoustic Emission. In Proceedings of the International Conference on Materials, Structures and Construction Technology—2017 (MSC 2017), Riga, Latvia, 27–29 September 2017.